The Seismic Record
A journal of the Seismological Society of America

The 14 December 2021 M_w 4.9 Offshore Jeju Island, Korea, Earthquake: Seismological Observation of an Intraplate Earthquake Provides Insight into Regional Seismotectonics

Won-Young Kim[1,2], Jun Yong Park[1], Min-Seong Seo[1], Young Oh Son[1], Hobin Lim[1], Sangwoo Han[1], and YoungHee Kim[*1]

Abstract

The M_w 4.9 Offshore Jeju Island, Korea, earthquake of 14 December 2021 is the most significant event that occurred close to the young intraplate volcano on the continental shelf south of the Korean Peninsula. About 185 small earthquakes occurred during nine days following the mainshock. We accurately located 39 events despite limited station azimuthal coverage. We found that the mainshock ruptured along a ~1.4 km long fault striking east–west (275°) and triggered two distinct clusters in the north–northeast direction. The mainshock is pure strike-slip faulting on the vertical plane. Its horizontal *P* axis strikes 50°, which differs substantially from the average trend of ~70° for earthquakes in the southern Korean Peninsula. However, it is consistent with the *P*-axes orientation of shallow earthquakes in the offshore western Kyushu and along Okinawa trough. The 2021 Offshore Jeju Island earthquake may be the first significant earthquake in southern Korea–East China Sea continental shelf to date, whose causative fault is well constrained by accurate aftershock locations and detailed space–time analysis of the earthquake sequence. This earthquake may represent intraplate deformation in response to the tectonic evolution of the Philippine Sea plate, which is manifested through volcanic activities.

Cite this article as Kim, W.-Y., Park, J. Y., Seo, M.-S., Son, Y. O., Lim, H., Han, S., and Kim, Y. (2022). The 14 December 2021 M_w 4.9 Offshore Jeju Island, Korea, Earthquake: Seismological Observation of an Intraplate Earthquake Provides Insight into Regional Seismotectonics, *The Seismic Record*. **2**(**2**), 107–117, doi: 10.1785/0320220012.

Supplemental Material

Introduction

A moderate-sized earthquake of magnitude M_w 4.9 occurred on 14 December 2021 offshore southwestern Jeju Island, South Korea. Twenty-one aftershocks (M_L 1.3–3.2) are reported by the Korea Meteorological Administration (KMA) within nine days following the mainshock. This earthquake occurred ~10 km offshore on the southwestern part of Jeju Island (Fig. 1). There was no reported damage on the island, but many residents, mostly around Seogwipo city (Fig. 1c), felt strong shaking with the maximum modified Mercalli intensity (MMI) V. The observed peak ground acceleration from the mainshock ranges from 6.89 (%*g*) at the nearest site MRD (Δ = 8.1 km, AZ = 79°) to 0.22 (%*g*) among eight stations with the accelerometer on Jeju Island. The shock was also felt in the southern provinces of the Korean Peninsula up to ~300 km from the epicenter (Fig. 1a). It is the largest earthquake in and around Jeju Island within a radius of ~200 km region since instrumental earthquake monitoring began in 1905 in Korea. The 14 December 2021 Offshore Jeju Island earthquake provides valuable ground-motion data to evaluate earthquake hazards around the southern coastal region of Jeju. The event offers seismic data to characterize source

1. School of Earth and Environmental Sciences, Seoul National University, Seoul, Republic of Korea, https://orcid.org/0000-0002-0005-9681 (W-YK); https://orcid.org/0000-0003-2244-0210 (JYP); https://orcid.org/0000-0001-7043-8938 (M-SS); https://orcid.org/0000-0001-9472-4314 (YOS); https://orcid.org/0000-0001-7510-4507 (HL); https://orcid.org/0000-0001-5832-7127 (SH); https://orcid.org/0000-0002-1111-632X (YHK); 2. Lamont-Doherty Earth Observatory, Columbia University, Palisades, New York, U.S.A.

*Corresponding author: younghkim@snu.ac.kr

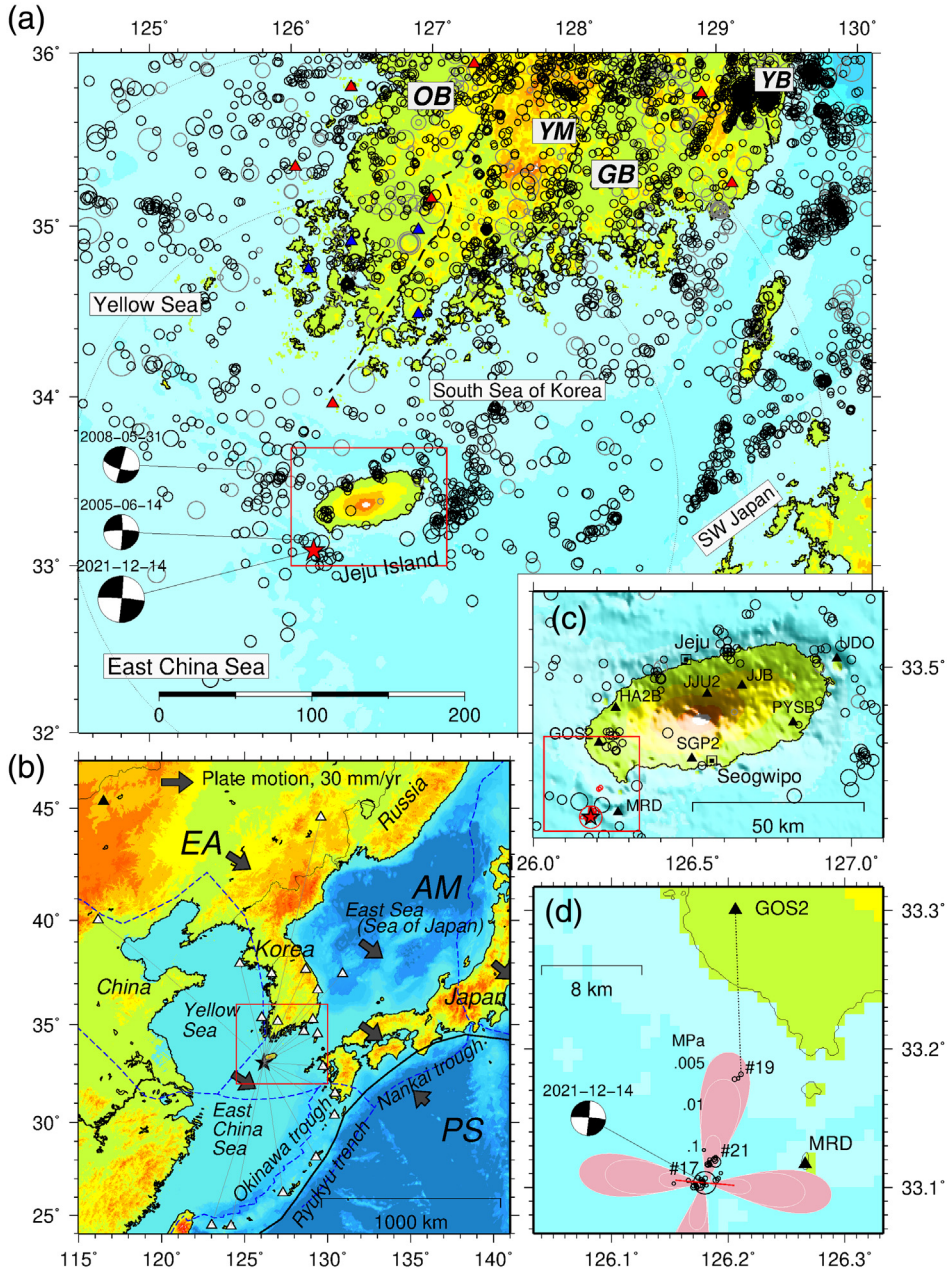

Figure 1. (a) Map showing topography and earthquakes around southern Korea, Jeju Island, and southwestern Japan. Earthquakes during 1900–2021 are plotted with circles, 2021 Offshore Jeju Island earthquake is shown as a red star, and seismic stations are shown as red triangles. The focal mechanism plots are of the 2021 Offshore Jeju Island earthquake (M_w 4.9) and two earthquakes that occurred close by on 14 June 2005 (M_w 3.8) and on 31 May 2008 (M_w 4.0). Major geologic units in the southern Korean Peninsula are drawn by thick dashed lines, from west to east: GB, Gyeongsang basin; OB, Okcheon fold belt; YB, Yeonil basin; and YM, Yeongnam massif. (b) Tectonic plates and their boundaries: AM, Amur; EA, Eurasian; PS, Philippine Sea; and YA, Yangtze. Blue dashed lines indicate plate boundaries suggested by Bird (2003). Seismic stations used for moment tensor analysis are plotted with white triangles. (c) Seismic stations on Jeju Island are plotted with triangles (Table S2). Red open circles are the 2021 Offshore Jeju Island earthquakes. (d) Detailed map of the 2021 Offshore Jeju Island earthquakes (circles). Mainshock fault trace is drawn as a solid red line. Three clusters of the earthquake sequence are indicated by #17, #19, and #21. The Coulomb failure stress changes by the mainshock are shaded in pink with white contour lines for their magnitudes (only the positive region).

properties and wave propagation paths in these stable continental regions (SCRs) with low seismicity.

In this article, we first briefly review the tectonic setting and seismicity of the region, and then present the source mechanism and focal depth of the mainshock. We conducted a waveform cross-correlation (WCC)-based earthquake detection, and precisely relocated the earthquake sequence to elucidate the causative fault and understand the detailed source process. This particular earthquake sequence is valuable to shed light on the seismogenesis and tectonics of this young intraplate volcanic island region (Fig. 1b).

Tectonic Setting

Around the southwestern Jeju Island, a lava flow of ~50 m thickness covers the surface, and ~100 m thick volcaniclastic deposits (Seogwipo formation) lie beneath the lava cover (Sohn and Park, 2004). Below the Seogwipo formation lies ~150 m thick unconsolidated sand and silt (Sohn and Park, 2004). The bedrock is a continuation of the Mesozoic Gyeongsang basin in the Korean Peninsula (e.g., Chough *et al.*, 2000; Fig. 1a).

In the late Eocene (~40 Ma), following the massive India–Eurasia collision, the extensional tectonics prevailed in the east–northeastern Asia, including the Korean Peninsula, until the middle Miocene (~14 Ma)

(e.g., Molnar and Tapponier, 1975). In much of southern Korea, a compressional stress regime developed in the late Miocene (~10 Ma), mainly due to plate-driving forces acting on the down-going slab along the Japan trench and inhibiting forces balancing them (Kearey and Vine, 1996).

In the early Pleistocene (~1.7 Ma), intraplate volcanism initiated on the submerged continental shelf in southern Korea around the present-day Jeju Island region and formed dispersed, small-volume basaltic tuff cones and rings (e.g., Sohn and Park, 2004; Sohn and Yoon, 2010). Beginning ~3.7 Ka, more voluminous lava eruptions formed a composite shield (e.g., Brenna *et al.*, 2015) that built Mt. Halla—a volcanic crater at the center of the island. The oval-shaped island (32 km by 75 km) is approximately 400–600 km from the plate boundaries—Okinawa and Nankai troughs (Fig. 1b). Hence, the island is formed as typical intraplate volcanism either by the mantle plume magmatism (e.g., Tatsumi *et al.*, 2005) or by the lithospheric extension (e.g., Anderson, 2000; Foulger, 2021). The east–west compressional stress since the late Miocene (~10 Ma) is still dominant in southern Korea (e.g., Kim *et al.*, 2010; Kim *et al.*, 2017). The 2021 Offshore Jeju Island event offers an opportunity to examine whether the same horizontal compressional stress is active around the epicentral region.

Seismicity in and around Jeju Island

We compiled a catalog of earthquakes around Jeju Island from 1900 to 2021 from KMA (1978–2021) and International Seismological Centre (ISC) (1900–2021) catalogs. Seismicity is dispersed, and most earthquakes occur offshore along the coastal regions of the island (Fig. 1a). The catalog is undoubtedly incomplete due to a sparse network in a continental shelf environment. A historical event with MMI VII was reported on 15 November 1670 at Jeju city (Fig. 1c; KMA, 2012).

There were no known earthquakes of magnitude >3.0 on the island, and no quake of magnitude exceeding 4.2 occurred in a broad region within a 200 km radius from Jeju Island, according to the catalog (see Fig. 1a). On the island, seismicity is characterized by clustered small earthquakes along the northern coastal regions revealed through the recent deployment of permanent stations on the island since 2002 (Fig. 1c). It is possible that the crust and uppermost mantle beneath the volcanic island may not allow brittle failure to take place due to the young volcanic region with high temperature (e.g., Song *et al.*, 2018).

Most earthquakes with $M_L > 2.5$ have occurred offshore in the west and east of the island as clusters with no known seismogenic faults (see Fig. 1a) and are typical SCR earthquakes away from plate boundaries. Notable events close to the epicentral area were the M_w 3.8 event on 14 June 2005, and M_w 4.0 event on 31 May 2008, which showed primarily strike-slip faulting mechanisms at 11–21 km depths (Rhie and Kim, 2010). Hence, the 14 December 2021 Offshore Jeju Island event with M_w 4.9 is a unique earthquake that occurred close to the young volcanic island.

Focal Mechanism and Depth of the Mainshock

Because the mainshock on 14 December 2021 is the largest known earthquake in and around Jeju Island, it is crucial to determine its focal mechanism and depth with certainty. Broadband KMA stations provided azimuthal coverage of ~110° covering the northeastern quadrant. Full Range Seismograph Network (F-net) and Japan Meteorological Agency network stations in western Japan provided coverage in the southeast. In addition, F-net stations on the Ryukyu Islands along the Okinawa trough provided coverage in the south (Fig. 1b). The Global Seismographic Network stations—INCN (489 km, AZ = 5°), BJT (1178 km, AZ = 314°), and MDJ (1314 km, AZ = 12°)—provided additional coverage. We selected 47 broadband stations in the distance ranges of 37 (SGP2) to 1314 km (MDJ) with wide azimuthal coverage for analysis (Fig. 1b).

We modeled three-component displacement records using the frequency–wavenumber integration method for a point source embedded in a 1D crustal velocity model, following the approach by Kim *et al.* (2010). The crustal model for southern Korea given by Kim and Kim (1983; KOR01) is used to calculate synthetic seismograms (Table S1, available in the supplemental material to this article). We modeled the complete waveform, including body waves and surface waves in the period between 10 and 33 s for regional records and between 2 and 20 s for local stations within 100 km (Fig. 2a). We inverted the focal mechanism parameters as a grid search through the whole parameter space of strike, dip, rake, and seismic moment (M_0) (Zhao and Helmberger, 1994).

We obtained a pure strike-slip faulting mechanism along near-vertical nodal planes striking north–south (5°) and east–west (275°), and horizontal *P* axis trending northeast–southwest (230°) (Fig. 2a). The focal depth is obtained by running the inversion for a range of focal depths with a 1 km interval and seeking the global minimum of the misfit. The inversions constrained focal depth between 10 and 14 km, with the fitting error minimum at 11 km depth (Fig. 2a).

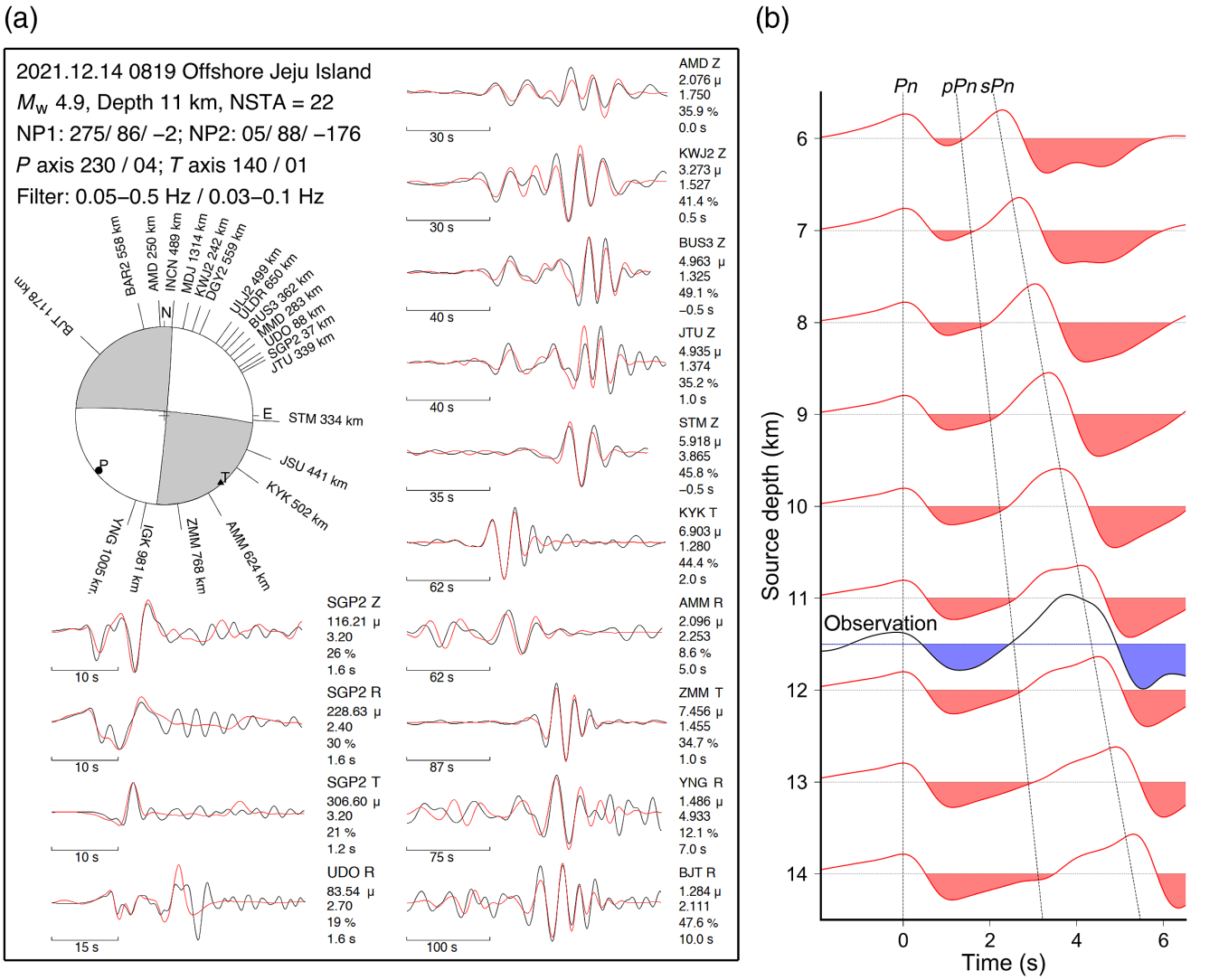

We employed the *Pn* phase and its depth phases, *pPn* and *sPn*, to estimate the focal depth independently from the regional moment tensor inversion. The *Pn* wave observed at an epicentral distance greater than ~270 km and stations in narrow azimuthal ranges of 32°–54° are selected for analysis, because *Pn* waves show consistent polarity and radiation pattern is the maximum along the azimuths. Vertical records from 26 stations are converted to displacement signal, bandpass filtered between 0.1 and 1.0 Hz, and stacked to enhance the weak *Pn* phases (Fig. 2b). We calculated synthetic seismograms of *Pn* and its depth phases, and compared them with the stacked record as shown in Figure 2b. The synthetics calculated from the model KOR01 for focal depths of 11 and 12 km fit the observed data with time delay best (*sPn*–*Pn* ~ 4.35 s), and we infer a focal depth of 11.5 km for the mainshock (Fig. 2b; Fig. S1).

Figure 2. (a) Comparison between observed (black lines) and synthetic (red lines) waveforms of the 14 December 2021 earthquake. Selected 14 traces out of 58 traces from 22 stations used are shown to illustrate wide azimuthal coverage and distance range. Synthetics are calculated for a focal depth of 11 km. Station code with component (Z = vertical, R = radial, and T = transverse components), the peak amplitude of observed records in micrometers (μ), the trace seismic moment in 10^{16} N · m from the amplitude ratio between the observed and synthetics, variance reduction in percentage, and time shift in seconds are indicated at the end of each trace. The mean seismic moment is $2.58 \pm 1.48 \times 10^{16}$ N · m from 58 traces. The average time shift from 58 traces is 1.2 ± 3.1 s, which suggests that the synthetics are slightly faster than the observed. (b) Comparison between the stacked observed *Pn* and its depth phases *pPn* and *sPn* (blue trace) and synthetic waveforms calculated for depth range from 6 to 14 km (red traces). The focal depth of the mainshock is constrained as 11.5 km.

2021 Offshore Jeju Island Earthquake Sequence

Following the mainshock on 14 December 2021, KMA reported 21 aftershocks within nine days, but no foreshocks were known or registered (Table 1). Those reported epicenters are spread in a rectangular area of 3.5 km × 8.0 km and hardly show any linear trend. We searched additional events using the WCC detection, and relocated the events precisely to delineate the mainshock fault plane and learn more details of the earthquake sequence.

Aftershock detection and hierarchical cluster analysis

We performed the WCC detection using 21 aftershocks reported by KMA as template events. We used vertical-component, continuous data in the frequency band of 5–25 Hz at three nearby stations on the island—MRD, GOS2, and HA2B (Fig. 1c; Table S2). The template traces start 0.5 s before *P* arrival and end 6, 8, and 13 s after *P* arrival for MRD, GOS2, and HA2B, respectively. The template traces include *P* and *S* waves, and have large signal durations and wide-frequency bandwidths that are key for a robust correlation detector (e.g., Kim *et al.*, 2018). We used a cross-correlation coefficient (Cc) of 0.3 as the detection threshold, which is about nine times the median absolute deviation for the cross-correlation traces obtained for each template during the first day (e.g., Daniels *et al.*, 2019). We detected 162 events with magnitude ranging from M_w −0.6 to 1.7 during nine days following the mainshock, but no event was found before the mainshock.

We employed a hierarchical cluster analysis of pairwise Cc of 76 selected events with a signal-to-noise ratio >5. Reordered Cc matrix shows three large submatrices (Fig. 3a), which are the clusters of events with similar waveforms.

We can first identify a submatrix of high Cc values, which includes seven events that are only detected by template event 19 (Fig. 3a). The events in the #19 cluster must be colocated with event 19, as the waveforms are nearly identical (Fig. 3b). The first event among the 28 detections occurred about 46 min after the mainshock, and most of them (26 events) happened within the first two and a half days. Hence, these multiplets must have occurred very close in space and time.

The next cluster with the high Cc is associated with event 21 (M_L 3.2)—the largest aftershock. #21 cluster has 17 events that are detected by the template events 18, 20, 21, and 23 (Fig. 3a; Table 1). The remaining 52 events formed a broad cluster with moderate Cc values and are denoted as the main cluster (Fig. 3a). The cluster consists of several subclusters of higher Cc values, as shown in the reordered Cc matrix (Fig. 3a). The largest subcluster within the main cluster is centered around the template event 17 (M_L 2.8) and includes two minor blocks: B block with events 13, 15, 17, and 22, and A block with events 4 and 10. These subclusters A and B form a larger cluster labeled as #17 (Fig. 3a). Hierarchical cluster analysis of the Cc matrix of aftershocks helps us to identify repeating events and to discern the spatiotemporal distribution of the earthquake sequence.

Location of 2021 Offshore Jeju Island earthquake sequence

We located the mainshock, two foreshocks on November 2021, and aftershocks to identify the fault plane. *P* and *S* arrival picks at eight stations are used to locate events using HYPOINVERSE (Klein, 1978). We observed a large-amplitude *S*-to-*P* converted phase (*Sp*) arrival on vertical record about 0.38 s ahead of strong *S* arrivals on horizontal seismograms at all stations in Jeju Island (see Fig. 3b,c). The *Sp* phase suggests presence of a low-velocity surface layer underneath stations. Synthetic seismogram calculations indicate that the *Sp* arrival time and amplitude can be modeled with about 2 km thick surface low-velocity layer with $V_S = 1.73$ km/s. We thus constructed a crustal velocity model (KOR02) by replacing the top 2 km of the two-layer velocity model—KOR01 (Table S1). We used the velocity model KOR02 for Jeju Island to locate the earthquake sequence (Figs. 1d and 4a).

The located events fall into three distinct groups consistent with the hierarchical cluster analysis of detected and catalog events. Most located events are around the mainshock and correspond to the main cluster in Figure 3a. These events are aligned east–west (see Fig. 4a) and consist of 24 events, including mainshock. We determined the moment magnitude for all 39 located events using source spectral analysis (Table 1; Fig. S4).

Twelve located events are clustered around the largest aftershock 21 (M_L 3.2), about 2.4 km from the mainshock. This cluster is identified as the #21 cluster in the cluster analysis (Fig. 3a). Three events are located around event 19 (M_L 1.4), about 11 km north–northeast from the mainshock (see Fig. 1d). Events in this group show highly similar waveforms (Fig. 3b). This group is the #19 cluster in the cluster analysis (Fig. 3a). The average horizontal location error is 1.24 ± 0.39 km (95% confidence level) for all the located events. However, the actual location uncertainty can be higher because

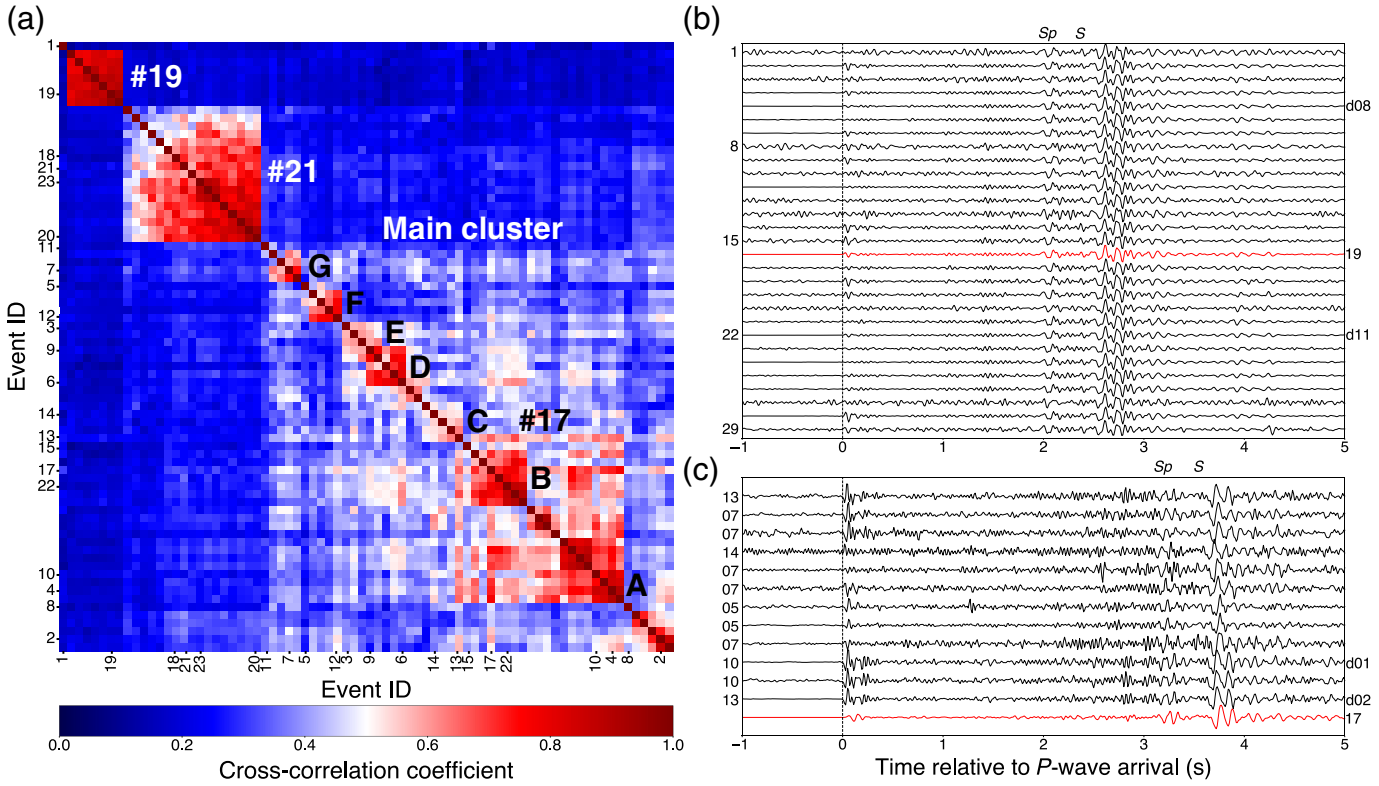

Figure 3. (a) Reordered cross-correlation coefficient (Cc) matrix of selected 76 event pairs. Average Cc values at stations MRD and GOS2 are used (Fig. 1d). The matrix shows three distinct clusters, which are #19 cluster, #21 cluster, and #17 cluster (= main cluster). Within the main cluster, seven subclusters are indicated as A through G. (b) Vertical records at GOS2 (13.2 km, AZ = 340°) from 28 detected events in the #19 cluster are plotted aligned to *P* arrivals. Event 19 is the red trace. *Sp* and *S* phases are indicated at the top. Located events are indicated with the event id at the end of traces. (c) Vertical records at GOS2 from 12 detected earthquakes during December 2016–November 2021 that preceded the mainshock. Event 17 is shown as the red trace to highlight similar *S*–*P* times of the detected events. Numbers at the start of each trace indicate the template event id used for detection.

of the large azimuthal gap of ~300° due to the offshore environment of the events (Fig. 1c,d).

Precise location of the earthquake sequence using double-difference (DD) relocation method

We relocated the aftershock sequence using the DD earthquake relocation method to constrain the fault plane (Waldhauser and Ellsworth, 2000). We first relocated the events using differential travel times of event pairs from the *P* and *S* arrival times (catalog) (Fig. 4b; Fig. S3). The majority of relocated events are aligned tightly along the east–west, consistent with the east–west-striking nodal plane (275°) of the focal mechanism solution (c.f., Figs. 2a and 4b). We measured the *P* and *S* differential times of the event pairs by WCC technique to reduce arrival-time picking errors.

The result of relocation using catalog and cross-correlation data shows that the aftershocks and two foreshocks of the main cluster are tightly aligned ~1.8 km along the east–west and extend to depths from 12.5 to 14 km with a mean depth of ~12.8 ± 1.64 km (Fig. 4d; Fig. S3). Ten events, including the two foreshocks around event 17, form a tight cluster at the shallow part of the fault patch (see Fig. 4c–f), and they appear to define the upper boundary of the mainshock rupture (Fig. 4d). Aftershocks and foreshocks of the main cluster are distributed on a 1.8 km × 1.4 km area (Fig. 4d), and they may define the mainshock source area of the earthquake sequence.

The northeast cluster (#21 cluster) is not on the same fault plane as the mainshock. Our calculation of the Coulomb failure stress change of the earthquake sequence suggests that the mainshock might have triggered this and #19 cluster (Fig. 4c,d; Fig. S5).

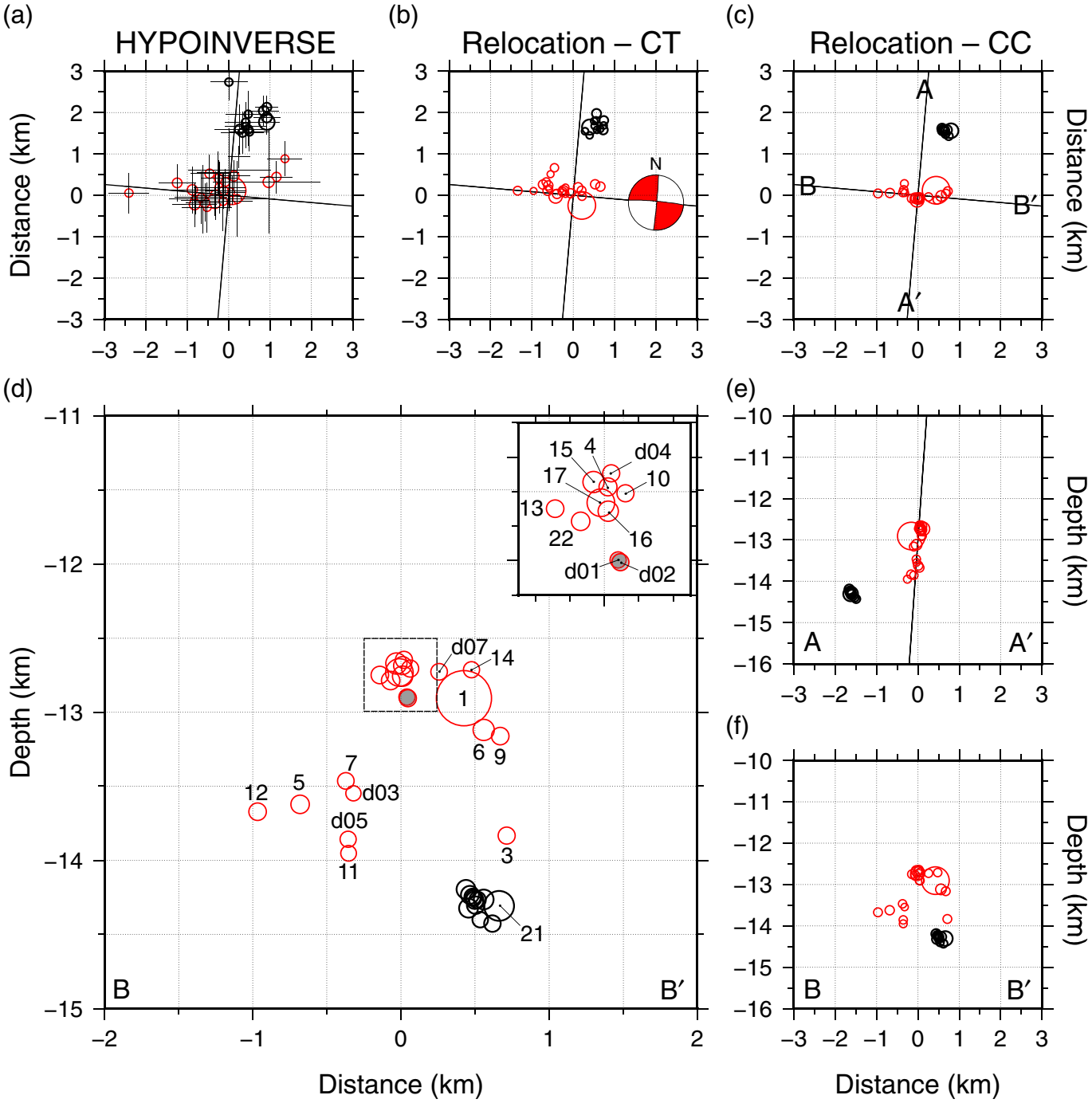

Figure 4. (a) Map view of 36 HYPOINVERSE locations with their horizontal and vertical location errors. (b) Map view of double-difference (DD) locations using only the phase data (event 8 not relocated). The mainshock focal mechanism is shown, and black lines indicate two nodal planes. The main cluster and the #21 cluster are shown as red and black circles, respectively. (c) Map view of DD locations using both phase and waveform cross-correlation (WCC) data (events 2 and 8 not relocated). (d) Detailed along-strike cross section (B–B′) of the DD locations constrained from the phase and WCC data. Two foreshocks are shown as filled gray circles. The mainshock source area is about 1.8 km × 1.4 km (vertical). (e) Across-strike cross section (A–A′) of the DD locations shown in panel (c). The vertical line through the hypocenters indicates a dip of 86° NE. (f) Along-strike cross section (B–B′) of the DD locations as panel (d) (see Fig. S3).

Detection of Repeating Earthquakes over Five Years in Stable Continental Margin

We further searched for foreshocks that might have occurred before the 2021 sequence using the WCC detection on the vertical records at GOS2 (22 km, AZ = 6°) that has been operated since early 2016. We detected 12 events during February 2016–November 2021 (Fig. S2). These 12 events have M_w 0.07–1.32 and are not on the KMA or ISC catalogs (see Table S3). Distribution in time is uneven, and no events were detected during 2018–2019. These events were detected by template events belonging to the main cluster, specifically subclusters #17 (events 10 and 13) and G (events 5 and 7) (Fig. 3a). High waveform similarity and nearly the same *S*–*P* time with event 17 (see Fig. 3c) indicate that these events must have originated from the same fault patch—the main cluster. Two large events among the 12 detected events have occurred on 1 November 2021 and belonged to subcluster #17 (d01 and d02 in Table 1). We thus assigned these two events as foreshocks of the 2021 earthquake sequence.

Those detected 12 small earthquakes spread in time up to five years apart (December 2016–November 2021) and have occurred offshore southwestern Jeju Island in a typical stable continental margin setting. All detected events must be repeating earthquakes that occurred within a few kilometers from each other based on their waveform similarity and high Cc (see Fig. 3c). Similar observations are reported for the central region of Korea by Kim and Kim (2014), for China (Schaff and Richards, 2011), and for Dover, Delaware (Kim *et al.*, 2018). These observations suggest that repeating earthquakes in SCRs with relatively low seismicity are common.

Discussion

The 14 December 2021 Offshore Jeju Island earthquake is the largest shock to have occurred close to the Jeju volcanic island since 1905. The mainshock occurred at about 12 km depth based on waveform modeling (11.0–11.5 km), single-event location (13.2 km), and relocation (12.9 km). Despite the large gap in station coverage, the nearest station at 8.1 km (MRD) provides some control on depth estimate.

The mainshock rupture is complex, as shown by two distinct source pulse arrivals of nearly equal amplitudes and a time difference of about 0.85 s (see Fig. S6). Although observation is limited in azimuthal coverage, each event has a simple triangular shape source time function with ~0.2 s duration (Fig. S6). The 2021 Offshore Jeju Island earthquake appears to be a compound earthquake, involving two events of similar size that occurred on nearby but different rupture surfaces close together in time, but with a delay such that their rupture times do not overlap (see Scholz, 2002).

Focal mechanism and regional variation of *P*-axis orientation

The moment tensor inversion for the mainshock using regional waveform data indicates that the horizontal *P* axis plunges 4° and trends southwest–northeast (50°), whereas the *T* axis trends northwest–southeast (140°). The *P*-axis orientation is the same as that of the 14 June 2005 event (*P*-axis trend = 50°) that occurred ~7 km north–northwest from the 2021 event (Rhie and Kim, 2010). This *P*-axis trend is substantially different from the broad-scale regional *P*-axis orientations in southern Korea where the *P* axes trend east-northeast–west-southwest (~70°; e.g., Park *et al.*, 2007; Kim *et al.*, 2010; Rhie and Kim, 2010). Most of the shallow earthquakes (<35 km) in the Global Centroid Moment Tensor catalog in western Kyushu Island and along the Okinawa trough show similar *P*-axis orientation comparable with the 2021 Offshore Jeju Island earthquake (see Fig. S7). We infer that the present-day broad regional stress field along the vast East China Sea–South Sea of Korea continental shelf is northeast–southwest-trending subhorizontal compressional stress.

Conclusions

The 14 December 2021 Offshore Jeju Island earthquake with M_w 4.9 is the largest earthquake that has occurred close to a young intraplate volcanic island near the Korean Peninsula. Mainshock mechanism is left-lateral, strike-slip faulting on vertical plane striking east–west with its *P*-axis trend differing by ~20° compared with earthquakes in the Korean Peninsula, but its *P* axis is more consistent with the orientation in offshore western Kyushu Island and along the Okinawa trough. This suggests that the northeast–southwest-trending compressional stress prevails in the vast continental shelf south of Jeju Island.

The earthquake sequence took place with three distinct clusters: the main cluster with two foreshocks (M_w 1.3–1.4) that occurred 45 days before the sequence, the mainshock, and over 120 aftershocks followed and distributed to the source area of 1.8 km × 1.4 km; the second cluster about 2.4 km north–northeast from the mainshock with 43 events; and the third cluster farther north-northeast from the mainshock with 29 events that show very similar waveforms as multiplets. The clusters are spatially separated in a direction in which Coulomb stress change is the maximum, suggesting that they have been triggered by the mainshock. Twelve small repeating

Table 1
Located Events of 14 December 2021 Offshore Jeju Island Earthquake Sequence

ID	Date (yyyy/mm/dd)	Time (UTC) (hh:mm:ss.s)	Latitude (°N)	Longitude (°E)	Depth (km)	Magnitude		*H* Error (km)
						M_L*	M_w	
01	2021/12/14	08:19:15.4	33.1033	126.1800	13.2	4.9	4.91	0.34
02	2021/12/14	08:29:05.3	33.1104	126.1937	14.5	1.3	1.11	0.42
03	2021/12/14	08:29:33.6	33.1040	126.1767	12.9	1.5	1.39	0.62
04	2021/12/14	08:36:55.0	33.1012	126.1705	12.5	1.7	1.65	0.34
05	2021/12/14	09:02:28.2	33.1070	126.1742	13.2	1.6	1.71	0.46
06	2021/12/14	09:23:11.2	33.1003	126.1703	13.0	1.7	2.10	0.54
07	2021/12/14	09:24:58.0	33.1061	126.1765	13.2	1.6	1.27	0.42
08	2021/12/14	10:02:39.8	33.1028	126.1533	13.4	1.5	1.11	0.49
09	2021/12/14	10:08:51.5	33.1064	126.1915	13.5	1.6	1.51	0.39
10	2021/12/14	10:14:46.7	33.1029	126.1794	12.7	1.6	1.45	0.37
11	2021/12/14	11:45:33.2	33.1052	126.1784	14.4	1.3	1.12	0.30
12	2021/12/14	13:02:01.9	33.1050	126.1658	13.7	1.5	1.54	0.45
13	2021/12/14	13:03:49.6	33.1033	126.1778	12.9	1.5	1.49	0.44
14	2021/12/14	13:36:34.1	33.1015	126.1726	12.0	1.3	1.18	0.82
15	2021/12/15	00:32:34.0	33.1022	126.1759	12.9	1.7	2.15	0.58
16	2021/12/15	00:32:35.3	33.1051	126.1895	13.8	2.0	2.03	1.25
17	2021/12/15	06:06:47.6	33.1010	126.1756	13.2	2.8	2.87	0.34
18	2021/12/15	15:16:54.0	33.1193	126.1889	14.5	1.7	1.93	0.32
19	2021/12/15	20:01:22.7	33.1817	126.2110	10.3	1.4	1.68	0.27
20	2021/12/16	12:03:03.0	33.1215	126.1891	14.1	1.4	1.58	0.28
21	2021/12/16	21:22:10.3	33.1183	126.1891	14.6	3.2	3.14	0.30
22	2021/12/18	14:50:50.2	33.1065	126.1804	12.5	1.9	1.66	0.38
23	2021/12/22	12:14:27.7	33.1206	126.1882	14.0	1.7	1.82	0.36
d01†	2021/11/01	19:59:31.0	33.0997	126.1735	12.9	1.3	1.25	0.60
d02	2021/11/01	20:24:54.4	33.1006	126.1729	12.7	1.5	1.44	0.46
d03	2021/12/14	16:24:32.8	33.1019	126.1720	13.4	0.9	0.86	0.63
d04	2021/12/15	00:31:19.2	33.1010	126.1777	13.0	1.4	1.36	0.71

Origin time, location, and depth are from HYPOINVERSE location; *H* error = crude horizontal location error estimate.

*M_L (local magnitude) reported by Korea Meteorological Administration for events 01–15 and 17–23; M_L from a regression relationship, $M_w = 1.03\ M_L - 0.06$, determined in this study for events d01–d16 and 16 (see Fig. S4c).

†Events with id d01–d16 are located events among the 174 detected events with small magnitude.

(Continued next page.)

Table 1 (continued)
Located Events of 14 December 2021 Offshore Jeju Island Earthquake Sequence

ID	Date (yyyy/mm/dd)	Time (UTC) (hh:mm:ss.s)	Latitude (°N)	Longitude (°E)	Depth (km)	Magnitude		*H* Error (km)
						M_L*	M_w	
d05	2021/12/15	02:00:05.0	33.1035	126.1697	13.6	1.2	1.20	0.56
d06	2021/12/15	02:55:29.7	33.1166	126.1842	14.3	1.5	1.53	0.40
d07	2021/12/15	02:58:09.9	33.1015	126.1814	13.0	1.3	1.27	0.91
d08	2021/12/15	05:56:06.4	33.1788	126.2085	10.9	1.3	1.23	1.00
d09	2021/12/15	08:18:46.9	33.1160	126.1827	14.2	1.5	1.49	0.51
d10	2021/12/15	23:22:01.8	33.1162	126.1845	14.3	1.3	1.32	0.48
d11	2021/12/16	08:30:47.5	33.1782	126.2055	10.2	1.7	1.74	0.51
d12	2021/12/16	21:38:44.8	33.1200	126.1842	14.1	1.4	1.34	0.56
d13	2021/12/17	00:02:15.0	33.1166	126.1821	14.2	1.8	1.80	0.60
d14	2021/12/17	02:06:01.1	33.1270	126.1792	15.9	1.1	1.03	0.46
d15	2021/12/17	23:02:24.0	33.1173	126.1834	14.0	1.2	1.17	0.51
d16	2021/12/18	12:24:06.5	33.1182	126.1835	14.0	1.3	1.26	0.50

Origin time, location, and depth are from HYPOINVERSE location; *H* error = crude horizontal location error estimate.

*M_L (local magnitude) reported by Korea Meteorological Administration for events 01–15 and 17–23; M_L from a regression relationship, $M_w = 1.03\ M_L - 0.06$, determined in this study for events d01–d16 and 16 (see Fig. S4c).

†Events with id d01–d16 are located events among the 174 detected events with small magnitude.

earthquakes are additionally detected based on their waveform similarities. These earthquakes with M_w 0.07–1.32 spread over five years and may represent a new form of seismicity in SCR.

Data and Resources

Earthquake catalogs of Korea and its surroundings were accessed from Korea Meteorological Administration (KMA) online catalog (https://www.weather.go.kr/w/eqk-vol/search/korea.do); International Seismological Centre (ISC), online bulletin (doi: 10.31905/D808B830). Global Centroid Moment Tensor (Global CMT) solutions were obtained from catalog available at https://www.globalcmt.org/CMTsearch.html. Waveform data from open stations of KMA (network code: KS) and Korea Institute of Geoscience and Mineral Resources (KIGAM) (network code: KG) were obtained from Incorporated Research Institutions for Seismology (IRIS) Data Management Center (DMC) at http://ds.iris.edu/SeismiQuery/by_network.html; Nonopen stations of KMA and KIGAM networks were acquired through written requests; Global Seismographic Network (GSN) and Japan Meteorological Agency (JMA) are obtained from Wilber3-IRIS-DMC (https://ds.iris.edu/wilber3/find_event); Full Range Seismograph Network (F-net) from the National Research Institute for Earth Science and Disaster Resilience (NIED), Japan (https://www.fnet.bosai.go.jp/top.php?LANG=en). The supplemental material for this article includes three tables, seven figures, and a reference list. All websites were last accessed in December 2021.

Data Availability Statement and Declaration

All data used in this study are available from the sources listed in Data and Resources.

Declaration of Competing Interests

The authors acknowledge that there are no conflicts of interest recorded.

Acknowledgments

This work was supported by Brain Pool Program through the National Research Foundation of Korea (NRF), funded by the Ministry of Science and ICT (2020H1D3A2A02047949). Y. K. acknowledges support from Creative-Pioneering Researchers Program through Seoul National University (SNU SRnD 3345-20160014). The authors would like to thank operators of the seismographic networks who provided waveform data in a timely fashion: Korea Meteorological Administration (KMA) and Korea Institute of Geoscience and Mineral Resources (KIGAM), Korea; National Research Institute for Earth Science and Disaster Resilience (NIED) and Japan Meteorological Agency (JMA), Japan; and Global Seismographic Network (GSN), United States. The authors thank Editor Keith D. Koper, Associate Editor Ruth Harris, and anonymous reviewers for helpful comments that improved this article. This is Lamont–Doherty Earth Observatory Contribution.

References

Anderson, D. L. (2000). The thermal state of the upper mantle; no role for mantle plumes, *Geophys. Res. Lett.* **27,** 3623–3626.

Bird, P. (2003). An updated digital model of plate boundaries, *Geochem. Geophys. Geosys.* **4,** no. 3, doi: 10.1029/2001GC000252.

Brenna, M., S. J. Cronin, G. Kereszturi, Y. K. Sohn, I. E. Smith, and J. Wijbrans (2015). Intraplate volcanism influenced by distal subduction tectonics at Jeju Island, Republic of Korea, *Bull. Volcanol.* **77,** 1–16.

Chough, S. K., S.-T. Kwon, J.-H. Ree, and D. K. Choi (2000). Tectonic and sedimentary evolution of the Korean Peninsula: A review and new view, *Earth. Sci. Rev.* **52,** 175–235.

Daniels, C., Z. Peng, Q. Wu, S. Ni, X. Meng, D. Yao, L. S. Wagner, and K. M. Fischer (2019). The 15 February 2014 M_w 4.1 South Carolina earthquake sequence: Aftershock productivity, hypocentral depths, and stress drops, *Seismol. Res. Lett.* **91,** 452–464.

Foulger, G. R. (2021). The plate theory for volcanism, in *Encyclopedia of Geology*, S. Elias and D. Alderton (Editor), Academic Press, Oxford, 879–890.

Kearey, P., and F. J. Vine (1996). *Global Tectonics*, Second Ed., Blackwell Science, Oxford.

Kim, S. J., and S. G. Kim (1983). A study on the crustal structure of South Korea by using seismic waves, *J. Korean Inst. Mining Geol.* **16,** 51–61.

Kim, W.-Y., and K.-H. Kim (2014). The 9 February 2010, Siheung, Korea, earthquake sequence: Repeating earthquakes in a stable continental region, *Bull. Seismol. Soc. Am.* **104,** 551–559.

Kim, W.-Y., H. Choi, and M. Noh (2010). The 20 January 2007 Odaesan, Korea, earthquake sequence: Reactivation of a buried strike-slip fault? *Bull. Seismol. Soc. Am.* **100,** 1120–1137.

Kim, W.-Y., M. Gold, J. Ramsay, A. Meltzer, D. Wunsch, S. Baxter, V. Lekic, P. Goodling, K. Pearson, L. Wagner, *et al.* (2018). The M_w 4.2 Delaware earthquake of 30 November 2017, *Seismol. Res. Lett.* **89,** 2447–2460.

Kim, Y., X. He, S. Ni, H. Lim, and S.-C. Park (2017). Earthquake source mechanism and rupture directivity of the 12 September 2016 M_w 5.5 Gyeongju earthquake, South Korea, *Bull. Seismol. Soc. Am.* **107,** 2525–2531.

Klein, F. W. (1978). Hypocenter location program HYPOINVERSE: Part I. Users guide to versions 1, 2, 3, and 4. Part II. Source listings and notes, *U.S. Geol. Surv. Open-File Rept. 78-694*.

KMA (2012). *Historical Earthquake Records in Korea (2∼1904)*, Korea Meteorological Administration, available at http://www.nims.go.kr/?sub_num=747&state=view&idx=440 (last accessed February 2022).

Molnar, P., and P. Tapponier (1975). Cenozoic tectonics of Asia: Effects of a continental collision, *Science* **189,** 419–426.

Park, J. C., W. Kim, T. W. Chung, C. E. Baag, and J. H. Ree (2007). Focal mechanisms of recent earthquakes in the southern Korean Peninsula, *Geophys. J. Int.* **169,** 1103–1114.

Rhie, J., and S. Kim (2010). Regional moment tensor determination in the southern Korean Peninsula, *Geosci. J.* **14,** 329–333.

Schaff, D. P., and P. G. Richards (2011). On finding and using repeating seismic events in and near China, *J. Geophys. Res.* **116,** no. B3, doi: 10.1029/2010JB007895.

Scholz, C. H. (2002). *The Mechanics of Earthquakes and Faulting*, Second Ed., Cambridge University Press, New York, 471 pp.

Sohn, Y. K., and K. H. Park (2004). Early-stage volcanism and sedimentation of Jeju Island revealed by the Sagye borehole, SW Jeju Island, Korea, *Geosci. J.* **8,** 73–84.

Sohn, Y. K., and S. H. Yoon (2010). Shallow-marine records of pyroclastic surges and fallouts over water in Jeju Island, Korea, and their stratigraphic implications, *Geology* **38,** 763–766.

Song, J. H., S. Kim, J. Rhie, S. H. Lee, Y. Kim, and T. S. Kang (2018). Imaging of lithospheric structure beneath Jeju Volcanic Island by teleseismic traveltime tomography, *J. Geophys. Res.* **123,** 6784–6801.

Tatsumi, Y., H. Shukuno, M. Yoshikawa, Q. Chang, K. Sato, and M. W. Lee (2005). The petrology and geochemistry of volcanic rocks on Jeju Island: Plume magmatism along the Asian continental margin, *J. Petrol.* **46,** 523–553.

Waldhauser, F., and L. Ellsworth (2000). A double-difference earthquake location algorithm: Method and application to the northern Hayward fault, California, *Bull. Seismol. Soc. Am.* **90,** 1353–1368.

Zhao, L. S., and D. V. Helmberger (1994). Source estimation from broadband regional seismograms, *Bull. Seismol. Soc. Am.* **84,** 91–104.

Manuscript received 16 March 2022
Published online 17 May 2022